Early version, also known as pre-print

Link to publication record in Explore Bristol Research
PDF-document

Global bifurcation investigation of an optimal velocity traffic model with driver reaction time

Gábor Orosz,* R. Eddie Wilson,† and Bernd Krauskopf‡

Bristol Centre for Applied Nonlinear Mathematics,
Department of Engineering Mathematics, University of Bristol,
Queen's Building, University Walk, Bristol BS8 1TR, United Kingdom
(Dated: Received: 27 January 2004)

We investigate an optimal velocity model which includes the reflex time of drivers. After an analytical study of the stability and local bifurcations of the steady state solution, we apply numerical continuation techniques to investigate the global behavior of the system. Specifically, we find branches of oscillating solutions connecting Hopf bifurcation points, which may be super- or subcritical depending on parameters. This analysis reveals several regions of multistability.

I. INTRODUCTION

The aim of this paper is to begin a systematic global investigation of the dynamics of car-following models of highway traffic, which include explicitly the reaction-time delay of drivers; see Helbing [1] for a recent large-scale review of the modeling of highway traffic.

Car-following models describe vehicles as discrete entities moving in continuous time and continuous one-dimensional space (lane-changing effects are ignored). Here we assume that vehicles have identical characteristics, that their positions are denoted by x_i, their velocities by v_i, and their relative displacements (called *headways*) by h_i [see Fig. 1].

Each car-following model consists of the kinematic conditions

$$\dot{h}_i(t) = v_{i+1}(t) - v_i(t)\,, \qquad (1)$$

where the dot denotes derivation with respect to time, together with a law that gives accelerations $\dot{v}_i$ as a function of stimuli. These stimuli are typically headways and velocities / relative velocities of nearby vehicles. A famous example is the so-called Optimal Velocity (OV) model introduced by Bando *et al.* [2], where the acceleration of the ith vehicle is given by

$$\dot{v}_i(t) = \alpha \left[\mathrm{V}\big(h_i(t)\big) - v_i(t) \right]. \qquad (2)$$

Here $\alpha > 0$ is known as the *sensitivity* and $\mathrm{V}(h)$ is known as the OV function. In this case the drivers' responses to stimuli are instantaneous, hence (1) and (2) constitute a system of ordinary differential equations (ODEs) for the vehicles' motions.

This paper is concerned with the OV model when drivers do not react instantaneously to their headways, so that the acceleration of the ith vehicle is given by

$$\dot{v}_i(t) = \alpha \left[\mathrm{V}\big(h_i(t - \tau)\big) - v_i(t) \right]. \qquad (3)$$

Here τ is the *reaction time* of the drivers, which is assumed to be the same for all drivers. (Note that τ is different from the characteristic *relaxation time* $T = 1/\alpha$ for adjustment of the vehicles' velocities, used by some authors [2, 3].) Together (1) and (3) give a system of delay differential equations (DDEs) for the vehicles' motions. Model (3) has recently been investigated with numerical simulation by Davis [4, 5]. The case where (the same) delay occurs both in the drivers' perceptions of their headway and in their perceptions of their own velocities, was considered by Bando *et al.* [6]. In our view, it is more realistic to suppose that drivers know their speed, i.e., they react to that instantaneously, but they react only to their headway via the delay τ.

The above OV models admit a one-parameter family of steady-state *uniform flow* solutions of the form

$$h_i(t) \equiv h^*, \quad v_i(t) \equiv \mathrm{V}(h^*)\,, \qquad (4)$$

for all i and for any constant $h^* > 0$. Previous studies in both ODE and DDE settings have been concerned with the linear stability computation of these uniform flow solutions and numerical simulation when the flow is unstable. The loss of linear stability of uniform flow solutions is widely accepted as a cause of traffic jams [1].

We begin in Sec. II by discussing details of the OV model. Then, as in previous papers, in Sec. III we give the linear stability calculation of the DDE system (1) and (3) for the uniform flow (4), and compute the neutral stability curves in the (h^*, α) plane. We then summarize the results of the weakly nonlinear analysis (for details, see [7]), which indicate that uniform flow may lose stability via either sub- or supercritical Hopf bifurcations. The presence of a subcritical bifurcation indicates the possi-

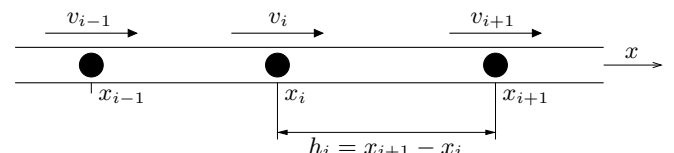———————
*Electronic address: `g.orosz@bristol.ac.uk`
†Electronic address: `re.wilson@bristol.ac.uk`
‡Electronic address: `b.krauskopf@bristol.ac.uk`

FIG. 1: Sequence of cars on a single-lane road showing their positions, velocities, and headways.

bility of the coexistence of stable solutions in a bistability region.

In Sec. IV we employ numerical continuation techniques to investigate efficiently the branches of oscillating solutions, far from bifurcation. The basic idea is to find a parameter value where the dynamics change qualitatively; for example, where the steady state becomes unstable. It is then possible to follow or continue the bifurcating oscillating solution or the bifurcation itself in several parameters; see Sec. IV for more information on numerical continuation.

While numerical continuation for ODE systems is well established (see, e.g., [8] and [9]), its implementation for DDE systems is much more recent. Our computations are done with the package DDE-BIFTOOL [10, 11], which is able to find and follow branches of steady and oscillating states irrespective of their stability.

To simplify these calculations and the exposition, we restrict ourselves to the situation with $n = 3$ cars on a closed ring. Nevertheless, this case is general enough to identify many general features; in particular, the existence of several regions of bistability where stable oscillating solutions coexist either with a stable uniform flow state, or with other nontrivial stable oscillating solutions. This is presented in a concise way in a two-dimensional parameter space to get a global overview of the regions of coexisting attractors. Furthermore, we consider a collision manifold, a stopping manifold, and their interaction with the two-dimensional bifurcation diagram (see Sec. IV C).

We note that bistability has been demonstrated by Igarashi et al. [12] (in the Newell model, which includes delay) and by Sugiyama and Yamada [3] for model (2) (that is, without delay) using numerical simulation of the initial value problem. However, numerical continuation techniques give us a more efficient way to characterize different regions of parameter space.

Finally, in Sec. V, we present practical conclusions and suggest possible extensions of this work.

II. DETAILS OF THE MODEL

We consider a single-lane model without overtaking, as shown in Fig. 1. To further simplify matters, we suppose that n vehicles are placed on a circular road of length L, so that

$$\sum_{i=1}^{n} h_i = L \,. \tag{5}$$

It follows that the nth car follows the first car and we are able to define $h_n = L - \sum_{i=1}^{n-1} h_i$ so that $\dot{h}_n = v_1 - v_n$. The equation of motion of the ith car is governed by the delay equation (3), and the *uniform flow equilibrium* (4) is given by

$$h_i(t) \equiv h^* = L/n \,, \quad v_i(t) \equiv \mathrm{V}(h^*) \,, \tag{6}$$

for all $i = 1, \ldots, n$, where $h^* = L/n$ is called the *average headway*. In this paper we focus mostly on the case $n = 3$.

The main task now is to identify desirable properties of the OV function $\mathrm{V}(h)$ and to estimate physical ranges for the parameters. Since $\mathrm{V}(h)$ describes the uniform flow equilibria, the following properties seem necessary from the modeling point of view:

(1) $\mathrm{V}(h)$ is continuous, nonnegative, and monotone increasing. [Drivers wish to travel forward and the desired velocity should increase smoothly as headway increases. Note that if $\mathrm{V}(h)$ were to attain negative values, there would exist unrealistic equilibria where vehicles reverse.]

(2) $\mathrm{V}(h) \to v^0$ as $h \to \infty$. [In the case of very large headway, the desired velocity should approach an upper limit v^0. This limit should be related to the legal speed limit.]

(3) There exists a *jam headway* $h_{\mathrm{stop}} \geq 0$ such that $\mathrm{V}(h) \equiv 0$ for $h \in [0, h_{\mathrm{stop}}]$. [If cars become too closely packed, then drivers want to come to a full stop.] In our view, one should take h_{stop} strictly positive. Firstly, this is because real vehicles have finite length, so that small positive headways correspond to collisions, and secondly because real traffic flows have a finite characteristic jam density at which traffic comes to a complete stop.

Note that a further advantage of choosing $h_{\mathrm{stop}} > 0$ is that maximum principles may be used to show that vehicles do not reverse under *any* (even dynamic) situations, for either model (2) or (3). However, it is still possible for vehicles to collide if other parameters are chosen appropriately.

In the original paper by Bando et al. [2], the OV function was given (in rescaled coordinates) by

$$\mathrm{V}_{\mathrm{B1}}(h) = \tanh(h - 2) + \tanh(2) \,. \tag{7}$$

It may be shown that this OV function satisfies each of the properties (1)–(3) above, although with $h_{\mathrm{stop}} = 0$, which we do not regard as suitable. The later paper [6] uses a dimensional OV function of the form

$$\mathrm{V}_{\mathrm{B2}}(h) = 16.8[\tanh\big(0.086(h - 25)\big) + 0.913] \,, \tag{8}$$

which was fitted to Japanese highway traffic data. Here h is measured in meters and $\mathrm{V}(h)$ in meters per second. It may be shown that $h_{\mathrm{stop}} \simeq 7.0319$ m and $v^0 \simeq 32.1384$ ms^{-1}. However, $\mathrm{V}_{\mathrm{B2}}(h)$ is a poor model for small headways since it is negative for $h \in [0, h_{\mathrm{stop}}]$. Thus properties (1)–(3) are satisfied by the OV function

$$\mathrm{V}_{\mathrm{B3}}(h) = \max[0, \mathrm{V}_{\mathrm{B2}}(h)] \,. \tag{9}$$

The numerical continuation method used in this paper requires the continuous differentiability of the model's right-hand side in terms of its dependent variables. Since $\mathrm{V}'_{\mathrm{B3}}(h)$ is not continuous at $h = h_{\mathrm{stop}}$, we must use a different OV function. Our goal is therefore to choose an OV function $\mathrm{V}(h)$ which satisfies properties (1)–(3) with $h_{\mathrm{stop}} > 0$ and for which $\mathrm{V}'(h)$ is continuous. The OV function should also have the correct S shape, i.e., we

Name	Symbol	Estimated values
Reaction/reflex time	τ	$0.5 - 2$ s
Relaxation time	$T = 1/\alpha$	$0.5 - 50$ s
Sensitivity	α	$0.02 - 2$ s^{-1}
Desired speed	v^0	$10 - 35$ ms^{-1}
Jam headway	h_{stop}	$2 - 15$ m
Average headway	$h^* = L/n$	...

TABLE I: Dimensional parameters with estimates of their ranges.

require $V'(h)$ to have a single maximum strictly to the right of h_{stop}.

Our approach is to first nondimensionalize (3). Since we assume that $\tau, h_{\text{stop}} > 0$, we may introduce the rescaled variables $\tilde{t} := t/\tau$ and $\tilde{h} := h/h_{\text{stop}}$. All speed-like quantities (including the OV function) have rescalings of the form $\tilde{v} = v\tau/h_{\text{stop}}$. To simplify notation we remove tildes, so that the rescaled version of (3) becomes

$$\dot{v}_i(t) = \alpha[V(h_i(t-1)) - v_i(t)]. \tag{10}$$

Table I suggests ranges for dimensional parameters and Table II gives the nondimensionalized counterparts.

Note that the equilibrium may still be written in the form (6) using rescaled quantities. The rescaled OV function $V(h)$ has the following properties:

(1) $V(h)$ is continuous, nonnegative, and monotone increasing.

(2) $V(h) \to v^0$ as $h \to \infty$.

(3) $V(h) \equiv 0$ for $h \in [0, 1]$.

The remainder of this paper uses the rescaled OV function

$$V(h) = \begin{cases} 0 & 0 \le h \le 1, \\ v^0 \dfrac{[(h-1)/s]^3}{1 + [(h-1)/s]^3} & h > 1, \end{cases} \tag{11}$$

which satisfies properties (1)–(3) above, has the requisite shape, and is smooth at $h = 1$. This OV function possesses two nondimensional parameters, namely v^0 and s. The former is determined by the dimensional version of v^0 and the applied rescaling. However, s is a wholly new parameter that describes how the OV function is stretched to the right of $h = 1$. In this paper we choose $s = 1$; the parameter s may be varied to shift the value of h at which $V'(h)$ attains its maximum.

Figures 2(a) and 2(b) compare (11) and its derivative (solid curves) with the the rescaled version of the OV

Name	Symbol and Definition	Estimated values
Sensitivity	$\tilde{\alpha} = \tau\alpha = \tau/T$	$0.01 - 4$
Desired speed	$\tilde{v}^0 = v^0\tau/h_{\text{stop}}$	$0.33 - 35$
Average headway	$\tilde{h}^* = h^*/h_{\text{stop}}$	...

TABLE II: Nondimensionalized parameters and their ranges.
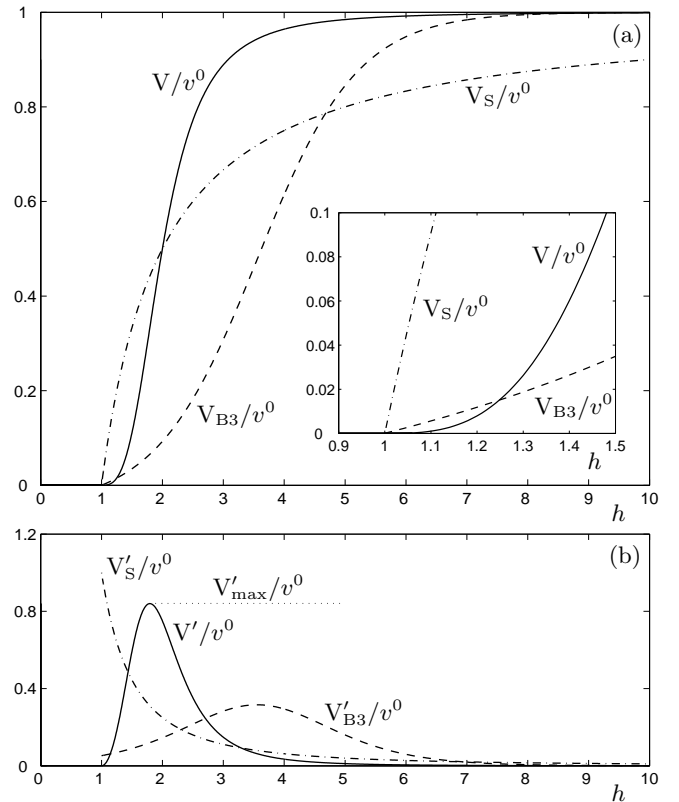

FIG. 2: Three different rescaled optimal velocity (OV) functions with an enlargement of the region around $h = 1$ (a), and the derivatives of the OV functions with respect to h (b).

function $V_{\text{B3}}(h)$ (9) (dashed curves). For comparison, we have also included a plot of the OV function

$$V_S(h) = v^0(1 - 1/h), \tag{12}$$

(dashed-dotted curves), which does not have an S shape for $h > 1$.

III. LOCAL BIFURCATIONS

Bando et al. [2, 6] and many subsequent papers have explained traffic jam formation in terms of the loss of linear stability of the equilibrium (6) to oscillations. Here we perform a linear stability analysis of (10), which is a DDE system and yields a more complicated characteristic equation than for ODE models.

Defining the perturbed solution

$$r_i(t) := h_i(t) - h^*, \tag{13}$$

and using the Taylor series expansion of $V(h)$ around h^* in the third order of $r_i(t)$, Eq. (10) gives the differential equation system

$$\dot{v}_i(t) = -\alpha v_i(t) + \alpha V'(h^*)r_i(t-1) + \frac{1}{2}\alpha V''(h^*)r_i^2(t-1) + \frac{1}{6}\alpha V'''(h^*)r_i^3(t-1). \tag{14}$$

In addition, the kinematic condition (1) can be written in the form

$$\dot{r}_i(t) = v_{i+1}(t) - v_i(t) \,. \tag{15}$$

In Eqs. (14) and (15) we model the circular road by identifying the $(n + 1)$-th vehicle with the first one.

We now consider the linear part of Eq. (14) and use the trial solution

$$r_i(t) = c_i e^{\lambda t} \,, \tag{16}$$

where $\lambda, c_i \in \mathbb{C}$, for $i = 1, \ldots, n$, to obtain the linear homogeneous equation

$$\Delta(\lambda) \begin{bmatrix} c_1 \\ \vdots \\ c_n \end{bmatrix} = 0 \,, \tag{17}$$

where $\Delta \in \mathbb{C}^n \times \mathbb{C}^n$. The characteristic equation is given by

$$\begin{aligned} D(\lambda) = \det \Delta(\lambda) &= [\lambda^2 + \alpha\lambda + \alpha V'(h^*)e^{-\lambda}]^n \\ &\quad - [\alpha V'(h^*)e^{-\lambda}]^n = 0 \,. \end{aligned} \tag{18}$$

To obtain the neutral stability curves, we substitute the critical eigenvalue $\lambda = i\omega$, $\omega \in \mathbb{R}$ into Eq. (18) and after taking real and imaginary parts, and some further calculation, we find that

$$\begin{aligned} V'(h^*) &= \frac{\omega}{2\cos(\omega - k\pi/n)\sin(k\pi/n)} \,, \\ \alpha &= -\omega \cot(\omega - k\pi/n) \,, \end{aligned} \tag{19}$$

where $k = 1, \ldots, n - 1$ is introduced by taking the nth root of unity.

By substituting (19) into Eq. (17), we may find the eigenvector components

$$c_i = \exp\left(i\frac{2\pi k}{n}i\right) \,, \tag{20}$$

which show that k is the discrete spatial wave number of oscillations along the ring. Note that we have omitted the discussion of the $k = 0$ (spatially independent) mode, since it violates the constraint

$$\sum_{i=1}^{n} r_i = 0 \,, \tag{21}$$

implied by (5).

Further, note that if (ω, k) solves (19), then so does $(-\omega, n - k)$. Here we chose to work with $\omega > 0$ and the full set of k. Alternatively, one could work with general $\omega \in \mathbb{R}$ and restrict attention to $k = 1, \ldots, n/2$ (even n) or $k = 1, \ldots, (n - 1)/2$ (odd n).

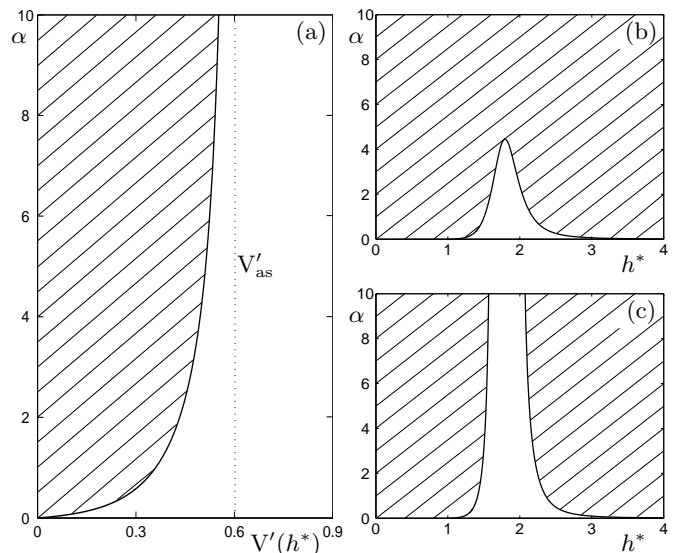Next, note that Eqs. (19) describe branches of curves in the $[V'(h^*), \alpha]$ parameter plane, which are parametrized

FIG. 3: Stability charts of the three-car system, where shading denotes the stable region. (a) Sensitivity α vs slope of the OV function $V'(h^*)$; (b) and (c) Sensitivity α vs average headway h^* for $v^0 = 0.6$ and for $v^0 = 0.8$, respectively. (This corresponds to $V'_{\max} \simeq 0.504$ and $V'_{\max} \simeq 0.672$, respectively).

by the frequency ω. Since we require $\omega, \alpha, V'(h^*) > 0$, for each k, we find a sequence of feasible intervals

$$\omega \in \left(-\frac{\pi}{2} + \frac{k\pi}{n} + 2l\pi, \, \frac{k\pi}{n} + 2l\pi\right) \cap \mathbb{R}^+, \, l = 0, 1, 2, \ldots \tag{22}$$

Each interval of ω traces out a different stability curve. Hence, we have a two-parameter family of stability curves described by $k = 1, \ldots, n - 1$ and $l = 0, 1, 2, \ldots$

We now focus on the case of $n = 3$ cars, where $h^* = L/3$ and wave numbers $k = 1, 2$ describe the same spatial pattern, i.e., one wave along the ring. It may be shown that the $k = 1$, $l = 0$ curve, which is parametrized by $\omega \in (0, \pi/3)$ and depicted in Fig. 3(a), is the left-most curve in the $[V'(h^*), \alpha]$ plane found by the above theory. This curve has a monotone shape with a vertical asymptote at $V'_{as} = \pi\sqrt{3}/9, \simeq 0.6046$.

By considering large α, one may apply the infinite dimensional Routh-Hurwitz criteria (see Stépán [13]), to show that the uniform flow equilibrium is stable to the left of this curve [shaded region in Fig. 3(a)] (all eigenvalues are situated in the left-half complex plane), and linearly unstable in a neighborhood of the right of the curve (there exist eigenvalues in the right-half complex plane). It is also possible to show that all other curves are destabilizing in that, as they are crossed from left to right, further eigenvalues move into the right-hand half plane. Hence, the $k = 1$, $l = 0$ curve divides the $[V'(h^*), \alpha]$ plane into regions where the uniform flow state is linearly stable or unstable. When crossing this curve from the stable to the unstable region, a complex conjugate pair of eigenvalues crosses the imaginary axis at $\pm i\omega$ and

a Hopf bifurcation takes place (see, e.g., [14–16]). Locally this gives a small amplitude oscillatory solution with frequency ω. The Hopf bifurcation is called supercritical if the oscillating solution is stable, and subcritical if it is unstable.

Our main interest is to convert Fig. 3(a) to a stability diagram in the average headway-sensitivity (h^*, α) plane, when we choose the OV function $V(h)$ given by (11) with $s = 1$. In this case $V'(h)$ has a single maximum over the interval $h \in [1, \infty)$ [solid line in Fig. 2(b)]. Hence, the (h^*, α) stability diagram can be obtained from the $[V'(h^*), \alpha]$ diagram by a kind of *nonlinear folding* about a vertical line whose abscissa corresponds to the maximum value V'_{max} of $V'(h)$ [see Figs. 3(b) and 3(c), where the shaded regions are stable]. For $V(h)$ given by (11) with $s = 1$, we have $V'_{max} = (2\sqrt[3]{2}/3)\, v^0, \simeq 0.8399\, v^0$. Hence, two qualitatively different cases of diagrams in the (h^*, α) plane are possible:

(1) In the first case shown in Fig. 3(b), the maximum value V'_{max} is to the left of the asymptote V'_{as} on the $[V'(h^*), \alpha]$ plane. This corresponds to $v^0 \lesssim 0.7198$. In this case, there is a critical sensitivity, α_{crit}; such that for $\alpha > \alpha_{crit}$, uniform flow equilibria are stable for all values of headway h^*. For $\alpha < \alpha_{crit}$, there is a bounded interval of headway h^* corresponding to unstable equilibria.

(2) In the second case shown in Fig. 3(c), the maximum value V'_{max} is to the right of the asymptote V'_{as} on the $[V'(h^*), \alpha]$ plane. This corresponds to $v^0 \gtrsim 0.7198$. In this case, for *any* value of α there is an unstable interval of headway h^*. It is not possible to stabilize all uniform flows by increasing α.

In the case without delay (that is, for $\tau = 0$), the stability region in the (h^*, α) plane takes the shape in Fig. 3(b) generally (see, e.g., [2, 3]). A situation like Fig. 3(c), where the unstable region is unbounded above, is not possible.

Returning to the model with delay, in either of the two cases above, decreasing α (or increasing v^0) increases the size of the unstable h^* interval, with the left-hand end point approaching 1, and the right-hand end point approaching $+\infty$, as $\alpha \to 0$.

When we consider different values of the scaling parameter s the stability charts shown in Figs. 3(b) and 3(c) do not change qualitatively. Here $V'_{max} = (2\sqrt[3]{2}/3s)\, v^0$, $\simeq (0.8399/s)\, v^0$ for general s, which only yields quantitative changes.

The qualitative picture for OV functions $V_{B3}(h)$ (9) and $V_S(h)$ (12) is similar, except for the following. For the function $V_S(h)$, the left-hand end of the unstable h^* interval is fixed at $h^* = 1$ for all α for which there is instability. For the function $V_{B3}(h)$, the left-hand end point of the unstable h^* interval attains $h^* = 1$ for positive α. These features are due to the discontinuities in the functions $V'_{B3}(h)$ and $V'_S(h)$ at $h^* = 1$ and the fact that $V'_S(h)$ also has its maximum at $h^* = 1+$.

We now briefly summarize the results of an analysis of the local Hopf bifurcation, more details of which may be found in Orosz and Stépán [7]. That technique allows one to determine the amplitude of the bifurcating orbit and whether the Hopf bifurcation is sub- or supercritical. The calculations are based on third-order Taylor expansion of the nonlinearity and give the first Fourier approximation of the oscillating solution, which is valid close to the bifurcation point.

Hopf calculations for DDEs are more complicated than for ODEs, because delay extends the dimension of the phase space to infinite (see Stépán [13], and Campbell and Bélair [17]). An added problem for the traffic model considered here is the translational symmetry along the ring, which implies a singularity in the Jacobian operator at the equilibrium, yielding further technical difficulties. This analysis is tractable only in the case of $n = 2$ cars, but it illustrates that the criticality of the Hopf bifurcation is highly dependent on the properties of the chosen OV function.

Denoting the value of h^* at the Hopf bifurcation point by h^*_{cr}, the Lyapunov coefficient can be computed as

$$\delta = \frac{V'''(h^*_{cr})}{8[V'(h^*_{cr})]^3 \alpha^2} \frac{(\alpha^2 + \omega^2)(\alpha^2 + \alpha + \omega^2)}{(2 + \alpha)^2 + (\alpha/\omega - \omega)^2}. \qquad (23)$$

When $\delta > 0$ (resp. $\delta < 0$) there is a subcritical (resp. supercritical) bifurcation. Since all other quantities are positive in the above expression, the sign of δ is determined by the sign of $V'''(h^*_{cr})$. This means that the third derivative of the OV function (whose sign is not obvious from a glance at the graph) plays an essential role in determining the global behavior of the system.

The amplitude of the headway oscillations can be computed as

$$A = 2\sqrt{-\frac{2V''(h^*_{cr})}{V'''(h^*_{cr})}(h^* - h^*_{cr})}, \qquad (24)$$

and the bifurcating oscillation in headway is described by the formula

$$\begin{bmatrix} r_1(t) \\ r_2(t) \end{bmatrix} = A \begin{bmatrix} -1 \\ 1 \end{bmatrix} \sin(\omega t), \qquad (25)$$

where the vector $[-1, 1]^T$ corresponds to the real part of (20) with $k = 1$.

IV. CONTINUATION ANALYSIS

In this paper we perform a bifurcation analysis of an optimal velocity traffic model with driver reaction time. The basic idea is to find a bifurcation (a parameter value where the dynamics changes qualitatively) and then follow or continue either the bifurcating solution or the bifurcation condition as parameters are changed. While it is not as straightforward as numerical simulation, bifurcation analysis is a powerful tool in that it allows one to map out the dynamics of a system in a systematic and
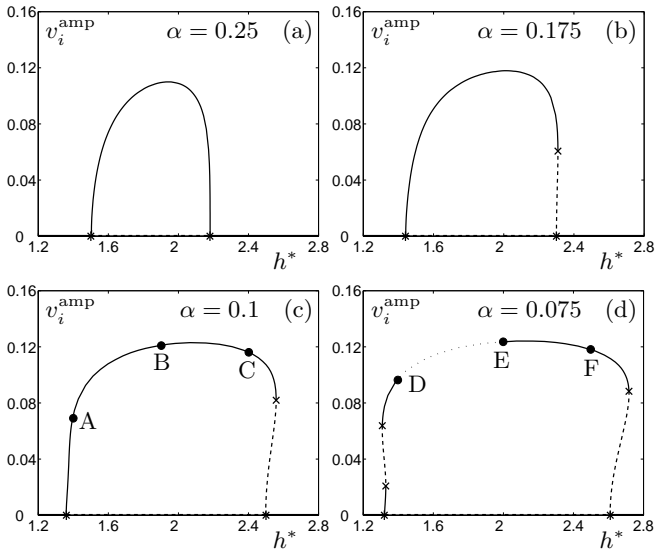
FIG. 4: Amplitude of oscillations of the velocity of the ith car vs average headway h^*. The horizontal axis represents the equilibrium state. Solid curves denote stable, and dashed curves denote unstable states; the dotted curve represents the collision region. The value of α is depicted in each panel (a)–(d) and $v^0 = 0.35$ in all panels.
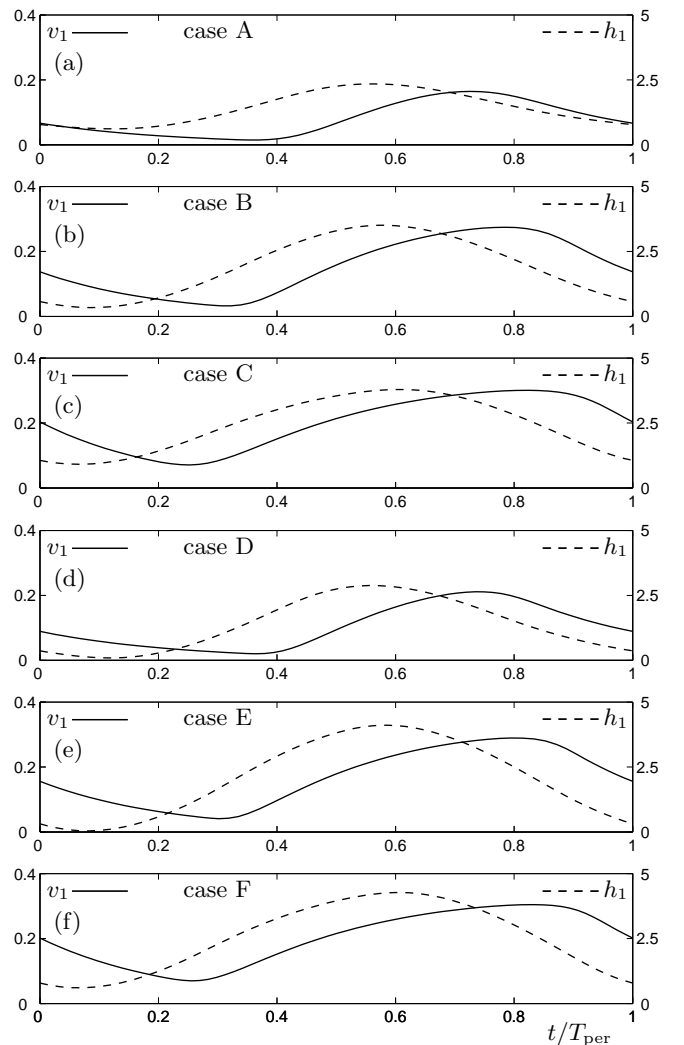

FIG. 5: Oscillations of the velocity of the first car over one period, shown as solid curves to the scale on the left-hand side, and oscillations of the headway of the first car over one period, shown as dashed curves to the scale on the right-hand side. Cases A–F correspond to the marks in Fig. 4.

efficient way. This approach is well established for systems modeled by ODEs and has been applied successfully in many areas of application (see, e.g., [14–16] as entry points to the extensive literature).

Dealing with a system with delay results in technical difficulties, due to the fact that the phase space of a DDE is infinite dimensional. For example, the linearizations around steady states and oscillating solutions are infinite-dimensional operators instead of matrices. This means that standard continuation software for ODEs, such as AUTO [9], cannot be used. However, recently, the package DDE-BIFTOOL, which works under Matlab, was developed by Engelborghs et al. [10, 11]. This software uses truncated matrices of appropriate sizes instead of operators, and is able to find and follow equilibria and oscillating solutions in DDEs even when they are unstable. Furthermore, it allows one to detect local bifurcations, where a solution changes its stability. In our model we find the Hopf bifurcation (where small amplitude oscillations are born) and the fold bifurcation of oscillating solutions (when two oscillating solutions of different stabilities merge and disappear).

DDE-BIFTOOL has not yet been used extensively in applications; examples of its use include the study of semiconductor laser systems (see Green and Krauskopf [18], and Haegeman et al. [19]). We use it here to investigate the dynamics of the smooth OV function (11) with $s = 1$ [solid line in Fig. 2]. Specifically, we follow branches of steady states and oscillating solutions and detect bifurcations when changing the parameter h^* for different values of α and v^0. The results are shown in Figs. 4–7. In the respective bifurcation diagrams the horizontal axis represents the equilibrium state. A solution is stable when plotted as a bold curve and unstable when dashed.

The branch of equilibria is unstable between two Hopf bifurcation points (denoted by *), in accordance with the results in Figs. 3(b) and 3(c). The bifurcating branches of oscillating solutions are represented by the amplitude of oscillation of the vehicles' velocities, through out $v_i^{amp} = (v_i^{max} - v_i^{min})/2$, which is the same for all cars ($i = 1, 2, 3$).

A. Oscillation and Collision

Let us first concentrate on the continuation results when the parameter α is changed and the parameter v^0 is fixed to $v^0 = 0.35$. This value of v^0 gives qualitatively
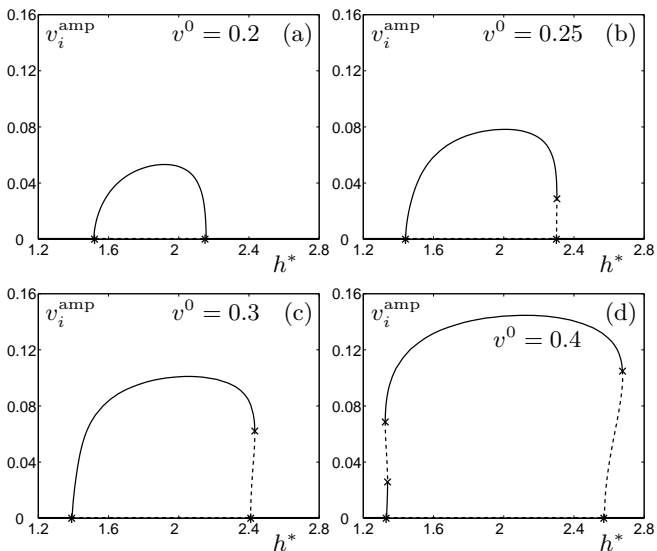
FIG. 6: Amplitude of oscillations of the velocity of the ith car vs average headway h^*. The horizontal axis represents the equilibrium state. Solid curves denote stable, and dashed curves denote unstable states. The value of v^0 is depicted in each panel (a)–(d) and $\alpha = 0.1$ in all panels.

FIG. 7: Stopping motion for $v^0 = 1.0$ and $\alpha = 1.0$. (a) Amplitude of oscillations of the velocity of the ith car vs average headway h^*. (b) Equilibrium state $V(h^*)$ (upper curve) and minimum of oscillations of the velocity of the ith car $v_i^{\min}$ (lower curve) vs average headway h^*. In panels (a) and (b) solid curves denote stable, and dashed curves denote unstable states. Panels (c)–(e) show oscillations of the velocity of the first car over one period as solid curves to the scale on the left-hand side, and oscillations of the headway of the first car over one period as dashed curves to the scale on the right-hand side. Cases G–I correspond to the marks in panels (a) and (b).

the stability behavior as shown in Fig. 3(b). For large values of α the two Hopf bifurcations are supercritical, as shown in Fig. 4(a). The computation of the bifurcating oscillating solution shows a stable oscillation branch above the unstable part of the equilibrium. We remark that the unstable part of the equilibrium disappears for extremely large α [see Fig. 3(b)]: the two Hopf bifurcation points come together and disappear, leaving the equilibrium stable for all h^*.

Decreasing α, the right Hopf point becomes subcritical, i.e., the right-hand side of the branch of oscillating solutions turn to unstable. Where the stable and unstable parts meet, a fold bifurcation takes place (marked by $\times$) as depicted in Fig. 4(b). Hence, a bistable area appears to the right of the right-most Hopf point, which means that the system tends to the oscillatory state or to the equilibrium, depending on the initial condition. We remark that this bistability has been found by numerical simulations in several car-following models [1], but we show that even a simple OV model as described here displays this effect for adequate values of parameters. When decreasing α further, the branch of oscillating solutions grows, as is visualized in Fig. 4(c), thus the bistable area becomes wider.

We marked some points A–C on the branch in Fig. 4(c) and display the associated time profiles in Figs. 5(a)–5(c). We show the velocity (solid curve) and the headway (dashed curve) over one oscillation period for the first car. (The plots are the same for all cars, except for a time shift.)

Note that in case A [Fig. 5(a)] vehicles nearly stop, and in case C [Fig. 5(c)] the maximum speed is close to
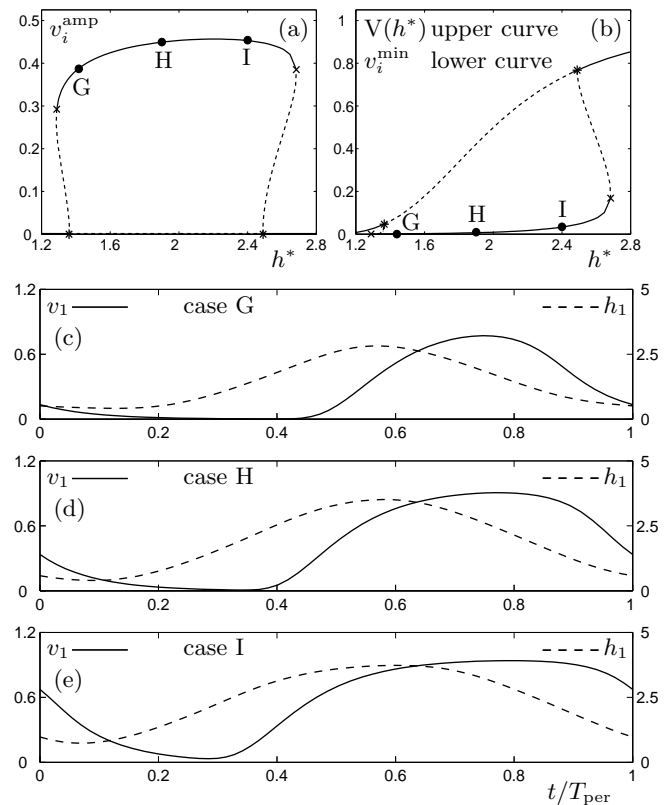
the desired speed v^0. Otherwise, there is no qualitative change between cases A–C. In addition, one can see that the oscillations of the headway are more harmonic than those of the velocity, that is, they are quite well approximated by the first term of the Fourier expansion.

Reducing α further, two interesting things happen as is visible in Fig. 4(d). First, an unstable part appears on the left-hand side of the branch of oscillating solutions (new dashed section) bounded by two fold bifurcations. This results in a second bistable region in the parameter h^*, where two different stable oscillations coexist, one with a smaller and one with a larger amplitude. As α is decreased further, the lower fold point tends to the left Hopf point, but does not reach it even when α is close to zero.

The second noticeable change in Fig. 4(d) is that the headway crosses zero during its oscillation along the dot-

ted section of the oscillating branch: cars move "through one another". Clearly the model is not valid in this situation, as collisions are not taken into account. We marked some points D–F on the branch of oscillating solutions and displayed the respective oscillations of the velocity and the headway in Figs. 5(d)–5(f). One can see in case D that the vehicles nearly stop and in case F they nearly reach the maximum speed [Figs. 5(d) and 5(f)]. Furthermore, in cases D and E [Figs. 5(d) and 5(e)] cars touch each other, because these points are on the edge of the collision region as shown in Fig. 4(d). Reducing α further, this collision section becomes larger and finally covers the entire stable part of the branch.

The height of the branch of oscillating solutions changes proportionally with v^0, because drivers want to reach the desired speed even during oscillations. Fixing $\alpha = 0.1$ and changing v^0, we obtain a series of bifurcation diagrams shown in Fig. 6. When increasing v^0, we observe the same qualitative changes as in Fig. 4. However, we did not encounter collisions, but they may occur at higher v^0. In fact, high desired speed, which is usually controlled by a given speed limit, can cause oscillations. We remark that in the above cases we showed that collisions may happen even for moderate v^0.

B. Stopping motion

We present the results in the range $\alpha \gtrsim 0.4$ of the sensitivity parameter to discover different bifurcation behavior. Note that here the relaxation time $1/\alpha$ is small, hence large acceleration can be achieved (the case of "rocket cars"). If we change v^0 in this regime of α (for example, for $\alpha = 1.0$), then we again get a series of growing branches of oscillating solutions and qualitatively the same branches as we obtained in Figs. 6(a)–6(c). However, instead of the behavior in Fig. 6(d), we experience the dynamics depicted in Fig. 7(a). On both sides of the branch of oscillating solutions, the same type of bistability appears, namely an unstable section of the branch of oscillating solutions between a fold and a subcritical Hopf bifurcation.

An important qualitative difference is that vehicles stop in one section of oscillations while there are no collisions [see time profiles Figs. 7(c)– 7(e) belonging to the marked points G–I of the oscillation branch]. This is due to the large acceleration. In fact, only for extremely large values of v^0, collisions appear in this regime of large α.

The stopping section is the largest in case G, is smaller in case H, and disappears in case I. However, in case H the maximum speed nearly reaches the desired speed. The collective motion of the system is a stop-and-go traffic jam: the congestion consisting of standing vehicles propagates upstream along the ring, because cars leave the jammed region at the front and enter at the back. Note that in case of three cars this jam is not pronounced, but the qualitative features of the oscillations are exactly the same as in the many-car case. We depict the equilibrium

state and the minimum of the oscillations in Fig. 7(b), where the minimum curve practically coincides with the horizontal axis in a large region in the parameter h^*. This shows that here, the stopping motions are typical system behavior.

C. Two dimensional bifurcation diagrams

The information concerning the dynamics of our model was presented in the previous sections, for example in Fig. 4, by plotting the amplitude of the oscillations as a function of the control parameter h^* for different fixed values of α (and fixed for v^0). In this way we detected points of bifurcation, where the dynamics changes qualitatively.

We now present this information in Fig. 8 in a more concise way as a two-dimensional bifurcation diagram in the (h^*, α) plane (for fixed v^0). Specifically, we show solid curves of Hopf bifurcation, dashed curves of fold bifurcation of oscillating solutions, gray curves of first collision, and dotted curves of first stopping. These curves divide the (h^*, α) plane into regions of qualitatively different behavior. In this representation, the diagrams we showed earlier correspond to horizontal cross sections for the fixed values of α that are indicated in Fig. 8 by dotted horizontal lines. We show the bifurcation diagram in the (h^*, α) plane for three representative values of v^0, namely for 0.35, 0.65, and 1.0.

The Hopf curves are the only curves that can be computed directly with DDE-BIFTOOL. Folds can only be detected by this software, and the fold curves were found by a script that detects a suitable number of individual fold points for (about 50) different values of the parameter α. In a similar approach, the collision curve was found by detecting points where the headway h_1 of the oscillating solution first crosses zero. Similarly, the stopping curve was found by detecting when the velocity v_1 first becomes (approximately) zero; in practice we used the criterion that $v_1 < 0.01$ because the velocity never actually attains zero in the numerical representation.

We now discuss the results in Fig. 8 in some detail. For $v^0 = 0.35$ [Fig. 8(a)] the Hopf curve is one single curve as in Fig. 3(b) (the top of the curve is not visible in the chosen window of α). There are fold curves on the right and on the left. The fold curve on the right starts at a degenerate Hopf point DH_r and approaches the h^* axis as shown. Above DH_r the Hopf bifurcation is supercritical and below DH_r it is subcritical. The region between the Hopf and the fold curve is thus identified as a region of bistability, where the equilibrium and a stable oscillating solution coexist. On the left-hand side, the Hopf bifurcation is always supercritical and the bistability appears via a cusp bifurcation where, two fold curves are born [see the inset of Fig. 8(a)]. The two fold curves end at the points $(0.0, 0.0167)$ and $(1.0, 0.0)$, respectively. The region between the two fold curves is a region of bistability. The Hopf curve divides this region into two subregions, in
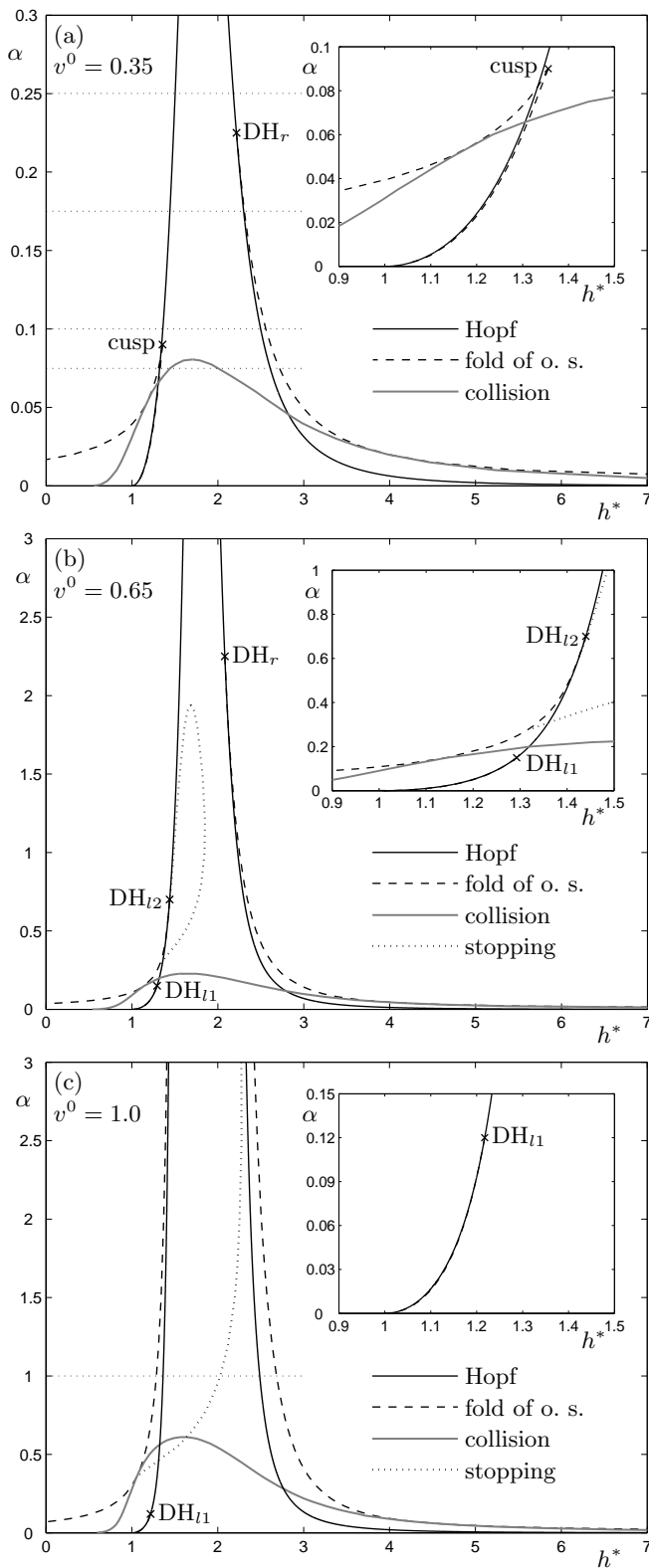
FIG. 8: Two-dimensional bifurcation diagrams for different values of v^0 as indicated. The horizontal dotted lines in panels (a) and (c) correspond to the values of α used in Figs. 4 and 7(a), respectively.

which the one on the left corresponds to the coexistence of an equilibrium and a stable oscillating solution, while the very small region on the right corresponds to the coexistence of two stable oscillating solutions; compare Fig. 4(d). For $v^0 = 0.35$ there is no stopping motion, but we find the gray curve of the first collision cutting across the bifurcation diagram. For any value of (h^*, α) below this curve collisions occur, which means that there are no collisions for $\alpha \gtrsim 0.0805$. The individual panels of Fig. 4 correspond to horizontal cross sections through Fig. 8(a) at the indicated values of α. In particular, Fig. 4(d) features collisions for values of h^* from the section between the two intersection points with the collision curve. This section becomes larger as α is decreased further. Where the collision manifold is tangent to the fold curve, collisions occur over the entire branch of stable oscillating solutions.

For $v^0 = 0.65$ [Fig. 8(b)] the bifurcation diagram is qualitatively the same as for $v^0 = 0.35$ except for two differences. First, the cusp point is gone and two degenerate Hopf points DH_{l1} and DH_{l2} are now the end points of the two fold curves on the left. (This change happens for a specific value of v^0 when the cusp point reaches the Hopf curve at $\alpha \simeq 0.4$.) The Hopf bifurcation is subcritical between these two degenerate Hopf points and supercritical otherwise. Coexisting stable oscillating solutions exist only in the tiny region between the Hopf curve and the fold curve below DH_{l1} (on the right side of the Hopf curve). In the much larger region between the other fold curve and the Hopf curve below DH_{l2} (on the left side of the Hopf curve), there is coexistence between the stable equilibrium and stable oscillations. The collision domain is qualitatively the same but it is now a bit larger; its top is at $\alpha \simeq 0.227$. The other new feature is the existence of stopping motion on the domain bounded by the left fold curve and the dotted stopping curve. The curve of first stopping appears to start at the point DH_{l2} and connect to a point on the left-most fold curve. This suggests that stopping motion is born when the cusp disappears.

For $v^0 = 1.0$ [Fig. 8(c)] there are now two vertical asymptotes of the two Hopf curves as in Fig. 3(c), meaning that the unstable area is now unbounded in α. Compared with the situation for $v^0 = 0.65$, the points DH_{l2} and DH_r moved up in α and out of our window, "dragging" the associated curves with them. In fact, these points have disappeared so that the fold curves and the stopping curve also now have vertical asymptotes. (We found that all vertical asymptotes develop for $v^0 \simeq 0.7198$.) In other words, Fig. 8(c) is qualitatively the same as Fig. 8(b) for, say, $\alpha \lesssim 0.7$. Notice how the stopping region is now much larger. The indicated horizontal section corresponds to Fig. 7(a), which indeed showed a large section of stopping motion. Furthermore, the collision domain is also much larger; its top is at $\alpha \simeq 0.61$.

When considering different values of the scaling parameter s, the only qualitative change is that the cusp point may be below the collision curve. For the OV functions

$V_{B3}(h)$ (9) or $V_S(h)$ (12), one can obtain similar branches of oscillating solutions as above, although the dynamics may be nonsmooth and thus DDE-BIFTOOL may run into difficulties.

V. CONCLUSION AND DISCUSSION

We presented a complete overview of the possible dynamics of the traffic model under consideration, in terms of all the relevant control parameters. To this end, we employed computational techniques and ideas from bifurcation theory. Our results show that even a simple delayed OV model with varying parameters can display many interesting features.

Specifically, we investigated the stability and the local Hopf bifurcations of the equilibrium, and used numerical continuation techniques to explore the bifurcations of the branches of oscillating solutions. We showed that, typically, an interval of h^* values exists in which the uniform flow solution is unstable. This region becomes larger when increasing the desired speed v^0 or the relaxation time $1/\alpha$. We then explored the oscillating solutions of the system by using continuation techniques, which showed that there are regions of bistability near the onset of oscillations; for example, between the uniform flow solution and oscillations. The different regions of behavior of the system were presented in a concise way in a bifurcation diagram in the (h^*, α) plane (for fixed v^0). In this bifurcation diagram we also identified the curves of (first) stopping and of (first) collision during an oscillating solution. While collisions occur for sufficiently small α, a region of stopping motion only occurs for sufficiently large v_0.

The next step is to use the approach taken here to perform bifurcation studies in more general situations. Here we kept to the case of three cars to present key phenomena in the simplest possible setting. A first exploratory investigation for four and five cars indicates that increasing the number of cars n results in no change in the qualitative structure of the stability diagram. While this number of cars may still appear small compared to real traffic situations, it nevertheless allows one to gain mathematical insight concerning the limit of a large numbers of cars. However, quantitative information concerning asymptotes changes and, as n is increased, we gain additional Hopf bifurcation curves for wave number values $k > 2$. Note that these extra bifurcation curves correspond to additional spectrum crossing into the right half plane when the uniform flow solution is already unstable. A bifurcation analysis of the n-car situation, especially the possibilities of interactions of different oscillating modes, is in progress.

We stress that numerical bifurcation techniques could be applied to extend the understanding of other car-following models incorporating delay (see Holland [20] for a list, and more recently, Lenz *et al.* [21], Nagatani [22], Wilson [23], and Sawada [24]). In some cases (see, e.g., Igarashi *et al.* [12], which discusses the Newell model), bistability has already been observed using numerical simulation techniques. The tools that were discussed here give more efficient methods for tracing out the key boundaries in parameter space (e.g., the characterization of bistability regions). Finally, we remark that chaos has been found in car-following models with delay by using numerical simulation; see Low and Addison [25], and Safonov *et al.* [26]. Numerical continuation techniques might, in the future, be applied to these models to gain concise information about the routes to chaos.

[1] D. Helbing. Traffic and related self-driven many-particle systems. *Reviews of Modern Physics*, 73(4):1067–1141, 2001.

[2] M. Bando, K. Hasebe, A. Nakayama, A. Shibata, and Y. Sugiyama. Dynamical model of traffic congestion and numerical simulation. *Physical Review E*, 51(2):1035–1042, 1995.

[3] Y. Sugiyama and H. Yamada. Aspects of optimal velocity model for traffic flow. In M. Schreckenberg and D. E. Wolf, editors, *Traffic and Granular Flow '97*, pages 301–318. Springer-Verlag, Singapore, 1998.

[4] L. C. Davis. Comment on "Analysis of optimal velocity model with explicit delay". *Physical Review E*, 66(3):038101, 2002.

[5] L. C. Davis. Modification of the optimal velocity traffic model to include delay due to driver reaction time. *Physica A*, 319:557–567, 2003.

[6] M. Bando, K. Hasebe, K. Nakanishi, and A. Nakayama. Analysis of optimal velocity model with explicit delay. *Physical Review E*, 58(5):5429–5435, 1998.

[7] G. Orosz and G. Stépán. Hopf bifurcation calculations in delayed systems with translational symmetry. Bristol Centre for Applied Nonlinear Mathematics Preprint 2004.02, University of Bristol, 2004. (http://www.enm.bris.ac.uk/anm/preprints/2004r02.html).

[8] R. Seydel. *From Equilibrium to Chaos: Practical Bifurcation and Stability Analysis*. Springer-Verlag, New York, 2nd edition, 1994.

[9] E. J. Doedel, A. R. Champneys, T. F. Fairgrieve, Yu. A. Kuznetsov, B. Sandstede, and X. Wang. AUTO97: Continuation and bifurcation software for ordinary differential equations. Technical report, Department of

Computer Science, Concordia University, 1997. (`http://indy.cs.concordia.ca/auto/`).

[10] K. Engelborghs, T. Luzyanina, and G. Samaey. DDE-BIFTOOL v. 2.00: a Matlab package for bifurcation analysis of delay differential equations. Technical Report TW-330, Department of Computer Science, Katholieke Universiteit Leuven, Belgium, 2001. (`http://www.cs.kuleuven.ac.be/~koen/delay/ddebiftool.shtml`).

[11] K. Engelborghs, T. Luzyanina, and D. Roose. Numerical bifurcation analysis of delay differential equations using DDE-BIFTOOL. *ACM Transactions on Mathematical Software*, 28(1):1–21, 2002.

[12] Y. Igarashi, K. Itoh, K. Nakanishi, K. Ogura, and K. Yokokawa. Bifurcation phenomena in the optimal velocity model for traffic flow. *Physical Review E*, 64(4):047102, 2001.

[13] G. Stépán. *Retarded Dynamical Systems: Stability and Characteristic Functions*, volume 210 of *Pitman Research Notes in Mathematics*. Longman, Essex, England, 1989.

[14] J. Guckenheimer and P. Holmes. *Nonlinear Oscillations, Dynamical Systems, and Bifurcations of Vector Fields*, volume 42 of *Applied Mathematical Sciences*. Springer-Verlag, New York, 1993.

[15] Yu. A. Kuznetsov. *Elements of Applied Bifurcation Theory*, volume 112 of *Applied Mathematical Sciences*. Springer-Verlag, New York, 2nd edition, 1998.

[16] S. H. Strogatz. *Nonlinear Dynamics and Chaos: With Applications in Physics, Biology, Chemistry, and Engineering*. Addison-Wesley, Reading, Massachuetts, 1994.

[17] S. A. Campbell and J. Bélair. Analytical and symbolically-assisted investigations of Hopf bifurcations in delay-differential equations. *Canadian Applied Mathematics Quarterly*, 3(2):137–154, 1995.

[18] K. Green and B. Krauskopf. Global bifurcations and bistability at the locking boundaries of a semiconductor laser with phase-conjugate feedback. *Physical Review E*, 66(1):016220, 2002.

[19] B. Haegeman, K. Engelborghs, D. Roose, D. Pieroux, and T. Erneux. Stability and rupture of bifurcation bridges in semiconductor lasers subject to optical feedback. *Physical Review E*, 66(4):046216, 2002.

[20] E. N. Holland. A generalized stability criterion for motorway traffic. *Transportation Research Part B: Methodological*, 32(2):141–154, 1998.

[21] H. Lenz, C. K. Wagner, and R. Sollacher. Multi-anticipative car-following model. *The European Physical Journal B*, 7(2):331–335, 1999.

[22] T. Nagatani. Traffic behaviour in mixture of different vehicles. *Physica A*, 284:405–420, 2000.

[23] R. E. Wilson. An analysis of Gipps's car-following model of highway traffic. *IMA Journal of Applied Mathematics*, 66(5):509–537, 2001.

[24] S. Sawada. Nonlinear analysis of a differential-difference equation with next-nearest-neighbour interaction for traffic flow. *Journal of Physics A*, 34:11253–11259, 2001.

[25] D. J. Low and P. S. Addison. A nonlinear temporal headway model of traffic dynamics. *Nonlinear Dynamics*, 16(2):127–151, 1998.

[26] L. A. Safonov, E. Tomer, V. V. Strygin, Y. Ashkenazy, and S. Havlin. Multifractal chaotic attractors in a system of delay-differential equations modeling road traffic. *CHAOS*, 12(4):1006–1014, 2002.